Frequency Diverse Array Spatial Data Focusing for High Precision Range-angle-based Geocasting

Guylian Molineaux, François Horlin, Philippe De Doncker, Julien Sarrazin

▶ **To cite this version:**

Guylian Molineaux, François Horlin, Philippe De Doncker, Julien Sarrazin. Frequency Diverse Array Spatial Data Focusing for High Precision Range-angle-based Geocasting. Conference GLOBECOM 2022, Dec 2022, Rio de Janeiro, Brazil. 10.1109/GLOBECOM48099.2022.10001165 . hal-03930137

HAL Id: hal-03930137

https://hal.sorbonne-universite.fr/hal-03930137

Submitted on 2 Feb 2023

HAL is a multi-disciplinary open access archive for the deposit and dissemination of scientific research documents, whether they are published or not. The documents may come from teaching and research institutions in France or abroad, or from public or private research centers.

L'archive ouverte pluridisciplinaire **HAL**, est destinée au dépôt et à la diffusion de documents scientifiques de niveau recherche, publiés ou non, émanant des établissements d'enseignement et de recherche français ou étrangers, des laboratoires publics ou privés.

Frequency Diverse Array Spatial Data Focusing for High Precision Range-angle-based Geocasting

Guylian Molineaux*†, François Horlin*, Philippe De Doncker*, Julien Sarrazin†
*OPERA – Wireless Communications Group
Université Libre de Bruxelles, 1050 Brussels, Belgium
†CNRS, Laboratoire de Genie Electrique et Electronique de Paris
Sorbonne Université, 75005 Paris, France
Univ. Paris-Saclay, CentraleSupélec, 91192 Gif-sur-Yvette, France

***Abstract*—A unified frequency diverse array (FDA) and spatial data focusing (SDF) system, or FDA-SDF, is proposed as a novel approach to perform spatially confined broadcasting of information, i.e. geocasting. It is shown that SDF processing exploits FDA range-angle-dependency more effectively than conventional power focusing implementations, resulting in improved spatial focusing precision and reduced array size. Additionally, the time-variance flaw in conventional FDAs is addressed and mitigated by introducing a generalized baseband FDA model. This paper describes the FDA-SDF system model in free space, including dedicated SDF precoding, beamsteering, and equalization, exploiting FDA multi-frequency transmission for 2-dimensional range-angle-based time-invariant geocasting. Simulations of the FDA-SDF system illustrate compatibility with conventional FDA frequency offset schemes and highlight degrees of freedom for geocast delivery zone manipulation. Finally, FDA-SDF's superior spatial precision is demonstrated: a 3-antenna FDA-SDF setup matches the radial and angular precision of a conventional FDA using, respectively, 13 and 23 antennas.**

***Index Terms*—Frequency diverse array (FDA), spatial data focusing (SDF), geocasting, single-antenna multi-carrier (SAMC).**

I. Introduction

Geocasting refers to the broadcasting of information that is exclusively retrievable by users within restricted geographical areas. As it targets a physical location, rather than individual users, centralized knowledge of a user's position is not required, avoiding potential privacy concerns. In internet-of-things or smart city environments, geocasting can provide location-dependent services or messaging to large and dynamic groups of mobile devices, e.g. for advertising and marketing, tourism, emergency signaling, traffic management, etc. [1]. At the network layer, geocasting is implemented through geographic routing algorithms that use location-based multicasting protocols to integrate geographic information into logical network addressing [2]. However, such protocols often require self-localizing nodes and struggle to trade-off delivery rate, overhead, and scalability. To alleviate these limitations, geocasting can be enforced at the physical layer. In this scenario, spatial focusing capabilities of base stations are exploited to restrict data retrieval to a geocast delivery zone where the bit error rate (BER) is sufficiently low.

This work was supported by the ANR GEOHYPE project, grant ANR-16-CE25-0003 of the French Agence Nationale de la Recherche, and carried out in the framework of COST Action CA20120 INTERACT. G. Molineaux is a FRIA grantee of the Fonds de la Recherche Scientifique – FNRS.

Beamforming is commonly employed to achieve the above scenario. It exploits constructive and destructive interference between signals transmitted from different antennas in an array to achieve spatial power focusing. As a result, sufficiently high signal-to-noise ratio (SNR), and thus sub-threshold BER, is obtained for specific directions only, where a geocast delivery zone is so created. While classical phased arrays (PAs) [3] are limited to beamforming in the angular domain, frequency diverse arrays (FDAs) achieve range-angle-dependent beamforming by adding small frequency offsets to the carrier frequency of each antenna [4]. Original linear FDAs, as in [4], that linearly increase the carrier frequency along the array, suffer from a range-angle-coupled beampattern that is continuous in space, thus failing to generate an isolated geocast delivery zone. Range-angle-decoupling of FDA beampatterns has been achieved by using nonlinear frequency offsets, such as logarithmic FDA [5] and symmetrical FDA [6]. However, beamforming's main limitation in geocasting context is the requirement of large arrays to obtain narrow beams, i.e. high precision. Additionally, it suffers from sidelobes of increased power (and hence decreased BER) that emerge and spread out from the main lobe, yielding a risk of potential data retrieval outside the geocast delivery zone.

Mitigation of the latter drawback is often attempted through the use of more complex or optimization-based frequency offsets for FDA, such as random FDA [7] or genetic algorithms [8]. Alternatively, in the context of physical layer security (PLS), directional modulation (DM) is regularly applied to beamforming schemes to secure communications in sidelobe directions. It has been integrated in both PA [9] and FDA [10] systems. Many of these approaches come, however, at the cost of increased design complexity and, moreover, fail to provide considerable precision improvements over classical PA and FDA schemes.

Beamforming and DM's spatial precision limitations are intrinsically related to their power focusing approach.

Spatial data focusing (SDF), on the other hand, fully releases the constraint of array radiation pattern manipulation for focusing. Instead, it performs distributed transmission of a global data stream over different antennas in an array, using uncorrelated and orthogonal signals. Its novelty lies in the realization that dedicated equalization at the receiver can exploit the different propagation conditions between the data sub-streams transmitted from each antenna to introduce a location-dependent symbol distortion that restricts correct recovery of information in space. In doing so, it increases precision, reduces array size, and minimizes complexity compared to power focusing techniques.

Time-based spatial data focusing (T-SDF) [11], which exploits the temporal dimension for signal orthogonality, has been shown to provide considerable spatial selectivity improvements over PA-based techniques. However, it is limited, just as PA itself, to focusing in the angular domain only. Range-angle-dependent SDF has been achieved by exploiting OFDM frequency resources in OFDM-based spatial data focusing (OFDM-SDF), both in free space [12] and multipath scenarios [13]. However, as frequencies are restricted to OFDM subcarriers, flexibility is limited and significant manipulation of the geocast delivery zone is challenging. On the other hand, this paper presents an FDA-based spatial data focusing (FDA-SDF) system that exploits FDA multi-frequency transmission for range-angle-dependent SDF. As it supports any type of FDA frequency offset configuration, it allows to exploit the additional degree of freedom of frequency offset design for geocast delivery zone manipulation. Thus, FDA-SDF simultaneously advances SDF and FDA literature by increasing, respectively, design flexibility over OFDM-SDF and focusing precision over conventional FDA schemes.

Additionally, the proposed FDA-SDF system provides novel opportunities to overcome the restricting time-variant nature of conventional FDA beampatterns revealed by [14]. Indeed, the inherent orthogonal nature of transmitted signals in SDF (and by extension FDA-SDF) ensures that radiation pattern manipulation and the resulting time-variance of conventional FDAs, as in [14], is avoided altogether. Similarly to [15], FDA-SDF is thus capable of employing a single-antenna multi-carrier (SAMC) receiver for the separate and time-invariant processing of FDA signals. However, [15] relies on low-pass filtering for signal extraction at the receiver, thus strongly reducing design flexibility by limiting the frequency offset range. On the other hand, FDA-SDF incorporates a generalized baseband FDA model, exploiting SDF's inherent signal orthogonality for time-invariant FDA operation, without frequency offset design restrictions.

The remainder of this paper is organized as follows. Section II presents the baseband FDA-SDF system model, which is expanded in Section III with beamsteering capabilities. Simulations and performance analyses are performed in Section IV. Finally, conclusions are drawn in Section V.

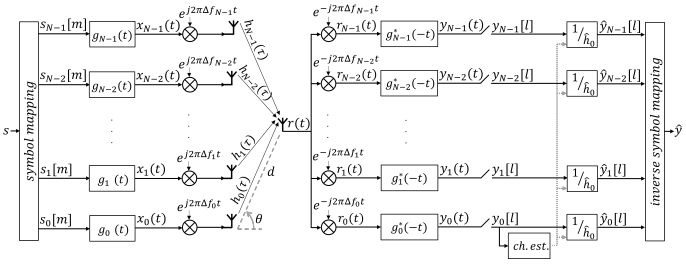

Fig. 1. FDA-based spatial data focusing baseband system model

II. System Model

Fig. 1 shows the system model for FDA-SDF. At the transmitter, a uniform linear array is used with N antennas and spacing b. In the context of FDA, the carrier frequency f_n at each antenna is defined by adding small frequency offsets Δf_n to a base carrier frequency f_c, i.e. $f_n = f_c + \Delta f_n$, with $\Delta f_n \ll f_c$. Where $n = -N_1, \dots, 0, \dots, N_2$ is the antenna index, with $N_1, N_2 \in \mathbb{N}$, $N = N_1 + N_2 + 1$, and the origin located at the antenna $n = 0$.[1] The antenna position along the array axis is then given by nb. While FDA models typically rely on the definition of a specific set of frequency offsets Δf_n, this paper presents a general system model compatible with any FDA frequency offset configuration. A receiver moves in a 2-dimensional plane around the transmitter, where its position is described by the polar coordinates (d, θ). They represent, respectively, the radial distance to the origin and the azimuth angle with respect to the array broadside direction.

A. Transmitter-side Signal Processing

In SDF context, information is transmitted in a distributed and orthogonal way over the different antennas in an array. For FDA-SDF in particular, symbols from an arbitrary symbol stream s at the transmitter's input are remapped to N sub-streams s_n. They are unique for each antenna n and carry complementary fragments of the information in s, i.e. the symbol mapping is disjoint and exhaustive. The proposed FDA-SDF system is compatible with any mapping scheme that satisfies these conditions, however, for simplicity, this paper maps successive symbols from s to the different sub-streams s_n in an alternating and cyclic manner, i.e. $s_n[m] = s[mN + n]$, with $m \in \mathbb{N}$ the sub-stream symbol index.

The symbols $s_n[m]$ are then modulated onto orthogonal time-shifted waveforms $g_n(t) = g(t - nT)$, where t is the time variable and $T = 1/B$ is the symbol period for a symbol rate B. The resulting baseband signal $x_n(t)$ to be transmitted from the n-th antenna is then given by

$$x_n(t) = \sum_m s_n[m] g_n(t - mT_a), \tag{1}$$

where $T_a = NT$ is the array symbol period, i.e. the time to have transmitted a single symbol from each antenna in

[1]Fig. 1 shows the common setup with $n = 0, \dots, N-1$, however the presented system model is compatible with alternative FDA models that employ an origin at one of the central antennas, e.g. [6].

the array. Thus, the symbols $s_n[m]$ are time-sequenced in accordance with the symbol mapping and the signals $x_n(t)$ become orthogonal in the time domain, enabling the distributed transmission of information over the array while mitigating interference between symbol sub-streams, as required for SDF.[2]

B. Baseband Frequency Diverse Array Channel Model

In the proposed baseband FDA system model, frequency up and down-conversion are each performed in 2 stages. At the transmitter, the signals $x_n(t)$ are first separately up-converted from baseband to an intermediate frequency (IF), equal to the frequency offset Δf_n of their respective antennas. Afterwards, they are collectively up-converted to radio frequency (RF) using the common base carrier frequency f_c, thus yielding the desired final carrier frequency f_n for each antenna n. Inversely, at the receiver, down-conversion from RF is first performed collectively using the common base carrier frequency f_c, followed by separate down-conversion from IF using each of the frequency offsets Δf_n. As a result, compared to former FDA models in literature, resource usage is reduced by requiring only a single RF local oscillator, flexibility for adjusting frequency offsets in practice is enhanced, and the RF propagation channel can be modeled in baseband by the channel impulse response (CIR) as in Fig. 1.

In this scenario, the signals transmitted from the n-th antenna are given by $x_n(t)e^{j2\pi\Delta f_n t}$. Being transmitted from different antennas, they are subject to distinct propagation conditions. Specifically, in a free space scenario, the channel for each antenna n is characterized by a unique propagation delay τ_n; contrarily, considering the close antenna spacing in the array, an identical complex amplitude α can be assumed for all channels. Under these conditions, the baseband CIR $h_n(\tau)$ corresponding to the n-th antenna, modeling the RF channel at the common base carrier frequency f_c, is given by

$$h_n(\tau) = \alpha\delta(\tau - \tau_n)e^{-j2\pi f_c\tau_n}, \tag{2}$$

where τ is the delay variable and $\delta(\cdot)$ the Dirac delta function. The total received IF signal $r(t)$ can thus be written as

$$\begin{aligned} r(t) &= \sum_n \left(x_n(t)e^{j2\pi\Delta f_n t}\right) * h_n(\tau) + z(t) && \text{(3a)}\\ &= \sum_n \alpha x_n(t-\tau_n)e^{-j2\pi f_n\tau_n}e^{j2\pi\Delta f_n t} + z(t), && \text{(3b)}\end{aligned}$$

where $*$ is the convolution operator and $z(t) \sim \mathcal{CN}(0, \sigma_z^2)$ models complex additive white Gaussian noise, with variance σ_z^2. The received signal (3b) is then further and separately down-converted with each of the FDA's frequency offsets. In particular, the received signal $r_v(t)$ after down-conversion with the frequency offset Δf_v is given by

$$\begin{aligned} r_v(t) &= r(t)e^{-j2\pi\Delta f_v t} && \text{(4a)}\\ &= \alpha x_v(t-\tau_v)e^{-j2\pi f_v\tau_v} \\ &\quad + \sum_{n\neq v} \alpha x_n(t-\tau_n)e^{-j2\pi f_n\tau_n}e^{j2\pi\Delta f_{nv}t} \\ &\quad + z_v(t), && \text{(4b)}\end{aligned}$$

where $z_v(t)$ is the noise after frequency down-conversion by Δf_v and $\Delta f_{nv} = \Delta f_n - \Delta f_v = f_n - f_v$ is the difference between the frequency offsets used for up and down-conversion. In contrast to FDA schemes in PLS context, in the envisioned geocasting scenario, cooperative receivers synchronized to the transmitter can be assumed, such that potential offsets between transmitter and receiver carriers can be omitted.

C. Receiver-side Signal Processing

Signal processing at the receiver consists of 2 parts. First, time-invariance is ensured by exploiting orthogonality upon demodulation of the received signals $r_v(t)$. Next, SDF equalization enforces the desired spatial focusing properties.

1) Time-variance Mitigation: In the received signal (4b) from the v-th receiver branch, time-variant phases $e^{j2\pi\Delta f_{nv}t}$ affect all signal components $x_n(t),\ n \neq v$, except the desired component $x_v(t)$, which is time-invariant. The latter can be extracted by exploiting the signal orthogonality introduced at the transmitter. To this end, demodulation of the signal $r_v(t)$ is performed through convolution with the matched filter $g^*(-t)$ of the time-orthogonal waveforms used at the transmitter. One finds that the demodulated signal $y_v(t)$ in the v-th branch at the receiver is then given by

$$\begin{aligned} y_v(t) &= r_v(t) * g^*(-t) && \text{(5a)}\\ &= \sum_n \alpha e^{-j2\pi f_n\tau_n}\Bigg\{\sum_m s_n[m] \\ &\quad \times \Big[\big(g(t-\tau_n-mT_a-nT)e^{j2\pi\Delta f_{nv}t}\big) * g^*(-t)\Big]\Bigg\} && \text{(5b)}\\ &\quad + z'_v(t),\end{aligned}$$

where $z'_v(t)$ is the noise after demodulation.

Thus, FDA time-variance impacts the matched filtering operation in (5b), potentially causing the symbols transmitted from antennas $n \neq v$ to generate inter-symbol interference (ISI) onto the desired symbols $s_v[m]$. However, in contrast to RF FDA models, it can be mitigated in the proposed baseband model by exploiting the additional degree of freedom offered by demodulation. Specifically, an appropriate choice of the filter $g(t)$ can ensure that orthogonality between signals transmitted from different antennas is preserved, despite the time-variant phases $e^{j2\pi\Delta f_{nv}t}$ in (5b). While multiple filters

[2]Note that by exploiting time-orthogonality in the transmitted signals $x_n(t)$, no restrictions apply to the choice of frequency offsets Δf_n. In contrast to previous SDF [12], [13] and SAMC FDA [15] schemes, that employ frequency-orthogonality.

may satisfy this condition, for the sake of simplicity, this paper adopts a rectangular filter shape for $g(t)$, defined as

$$g(t) = \begin{cases} 1/\sqrt{T} & |t| < T/2 \\ 0 & |t| \geq T/2. \end{cases} \tag{6}$$

Then, by sampling the demodulated signal $y_v(t)$ at $t = \tau_0 + vT + lT_a$, the l-th symbol from the v-th received symbol sub-stream $y_v[l]$ can be extracted, free from ISI caused by symbols transmitted from antennas $n \neq v$. One finds

$$y_v[l] = \alpha s_v[l] e^{-j2\pi f_v \tau_v} + z'_v[l], \tag{7}$$

where $z'_v[l]$ is the sampled noise. Additionally, a narrowband scenario was assumed, i.e. $\tau_n - \tau_0 \ll T$, such that sampling offsets due to the delay difference between τ_n and τ_0 can be neglected. Thus, each receiver branch v in the proposed baseband FDA model successfully extracts the symbols transmitted from the corresponding v-th antenna at the transmitter, affected by the correct and desired time-invariant FDA phase shift.[3]

2) Spatial Data Focusing Equalization: Following a conventional SDF approach, channel estimation at the receiver is performed exclusively for a designated reference channel and this unique estimation is employed for equalization of all channels. More specifically, for FDA-SDF, the reference channel is defined to correspond to the reference antenna at the origin, i.e. $n = 0$. It is estimated based on a traditional single-input single-output preamble transmission from the reference antenna.

For interpretation purposes of this equalization process, the following notations are adopted. The delay difference between the n-th channel and reference channel is written as $\Delta\tau_n = \tau_n - \tau_0$. Similarly, by assuming – without loss of generality – that the reference channel carrier frequency is equal to the base carrier frequency, i.e. $f_0 = f_c$, the frequency difference between the n-th channel and the reference channel is given by $\Delta f_n = f_n - f_c = f_n - f_0$. Simple zero forcing equalization of the received symbols (7), using the reference channel estimation, then yields the following expression for the m-th equalized symbol from the n-th channel

$$\hat{y}_n[m] = s_n[m] e^{-j2\pi f_0 \Delta\tau_n} e^{-j2\pi \Delta f_n \tau_n} + \hat{z}_n[m], \tag{8}$$

where $\hat{z}_n[m]$ is the noise sample after equalization.

Thus, the equalized symbols (8) in FDA-SDF are subject to a residual phase shift induced by the delay and frequency offset, $\Delta\tau_n$ and Δf_n, of the equalized channel with respect to the reference channel. As such, perfect recovery of the corresponding information is achieved only when this phase shift is equal to zero or an integer multiple of 2π, i.e.

$$-2\pi f_0 \Delta\tau_n - 2\pi \Delta f_n \tau_n = k2\pi, \quad k \in \mathbb{Z}. \tag{9}$$

[3]Note that sampling extracts a single unique symbol with index $m = l$ from antenna $n = v$. As such, without loss of generality, the symbol index m and antenna index n identifying transmitted symbols suffice to unambiguously identify received symbols as well. The indices l and v can thus be omitted in the remainder of this paper.

Under paraxial approximation ($b \ll d$), the delay τ_n and the delay difference $\Delta\tau_n$ can be expressed as a function of the receiver coordinates (d, θ) as follows

$$\tau_n = \frac{d}{c} - n\frac{b}{c}\sin\theta \tag{10a}$$

$$\Delta\tau_n = -n\frac{b}{c}\sin\theta, \tag{10b}$$

where c is the speed of light. As a consequence, compliance to the phase condition (9) depends on the receiver position, such that the residual phase shift imposed by SDF on the equalized symbols (8) enforces a restricted spatial access to the transmitted information. In particular, by substituting (10a) and (10b) for τ_n and $\Delta\tau_n$ in (9), one finds that the coordinates of the positions where the information transmitted from the n-th antenna is perfectly recovered satisfy

$$d = nb\frac{f_n}{\Delta f_n}\sin\theta - \frac{c}{\Delta f_n}k. \tag{11}$$

The entire received symbol stream $\hat{y}$ is reconstructed by inverting the transmitter-side symbol mapping, i.e. $\hat{y}[mN + n] = \hat{y}_n[m]$. Perfect recovery of the entire data stream is thus only achieved when each symbol sub-stream $\hat{y}_n$ is received without residual phase shift distortion, i.e. at the geographical coordinates where the curve (11) from each antenna n intersects with all others. As a result, the residual phase shifts on the equalized symbols (8) are collectively negligible for all antennas n around this position only, establishing a spatial region – the geocast delivery zone – where the bit error rate (BER) remains below a threshold and where information is thus exclusively retrievable. The exact geographical properties (e.g. size, shape, periodicity, etc.) of the geocast delivery zone are determined by the choice of frequency offsets Δf_n. A detailed study of this relationship is beyond the scope of this paper, however Section IV illustrates the fundamental degrees of freedom in frequency offset definition that can be exploited to manipulate the FDA-SDF geocast delivery zone.

III. Beamsteering

Section II describes FDA-SDF's ability to restrict correct recovery of transmitted information to a spatially confined geocast delivery zone. However, its exact location cannot be actively manipulated. Steering of the geocast delivery zone towards an arbitrary target position $(d^{steer}, \theta^{steer})$ is enabled by adding a steering phase φ_n^{steer} to the symbol sub-stream for each antenna n following symbol remapping, such that the corresponding transmitted symbols become $s_n[m]e^{j\varphi_n^{steer}}$. Following an analogous reasoning to Section II, the equalized FDA-SDF symbols received from the n-th channel then become

$$\hat{y}_n[m] = s_n[m] e^{j\varphi_n^{steer}} e^{-j2\pi f_0 \Delta\tau_n} e^{-j2\pi \Delta f_n \tau_n} + \hat{z}_n[m]. \tag{12}$$

Consequently, the residual phase shift condition ensuring perfect symbol recovery from the n-th antenna becomes

$$\varphi_n^{steer} - 2\pi f_0 \Delta\tau_n - 2\pi \Delta f_n \tau_n = k2\pi, \quad k \in \mathbb{Z}, \tag{13}$$

from which the steering phase can be isolated, yielding

$$\varphi_n^{steer} = 2\pi\big[k + f_0\Delta\tau_n + \Delta f_n\tau_n\big]. \tag{14}$$

Compliance to the steered residual phase condition (13) should be ensured at the target position. Thus, the final expression for the steering phase to be added to the symbols transmitted from the n-th antenna is found by evaluating (10a) and (10b) at the target coordinates $(d^{steer}, \theta^{steer})$ and substituting them for τ_n and $\Delta\tau_n$ in (14). One finds

$$\varphi_n^{steer} = 2\pi\left[\Delta f_n\frac{d^{steer}}{c} - f_n\frac{nb}{c}\sin\theta^{steer}\right], \tag{15}$$

where the integer k was set to zero as it modifies the steering phase by multiples of 2π only. By introducing this expression (15) in the steered residual phase condition (13) and additionally substituting (10a) and (10b) for τ_n and $\Delta\tau_n$, one finds that, in the presence of steering phases, the positions where information transmitted from the n-th antenna is perfectly recovered satisfy

$$d = d^{steer} + nb\frac{f_n}{\Delta f_n}\left[\sin\theta - \sin\theta^{steer}\right] - \frac{c}{\Delta f_n}k. \tag{16}$$

Intersection of this curve from each antenna n with all others is indeed obtained at $(d^{steer}, \theta^{steer})$ for $k = 0$, such that a geocast delivery zone is successfully established at the desired location.

IV. Simulations and Performance Evaluation

The proposed FDA-SDF scheme is simulated using the following system parameters. The transmitted symbols are defined by mapping a bitstream of length 10^5 onto a 16 QAM constellation. Steering phases are configured according to a steering range and angle of, respectively, $d^{steer} = 75$ m and $\theta^{steer} = 15°$. A base carrier frequency and symbol rate of, respectively, $f_c = 3.6$ GHz and $B = 50$ MHz are used. Half-wavelength antenna spacing is employed in the array, i.e. $b = \lambda_c/2$, with λ_c the base carrier wavelength, while the number of antennas N is varied. The signal-to-noise ratio (SNR) is fixed to 25 dB.

TABLE I
Frequency Offset Schemes for FDA-SDF Simulation

FDA Type	Frequency Offset Values	Antenna Index Range
symm. linear [6]	$\Delta f_n = \lvert n\rvert\Delta f$	$n = -\frac{N-1}{2}, \ldots, \frac{N-1}{2}$
alt. linear	$\Delta f_n = \begin{cases} +n\Delta f & n \text{ odd} \\ -n\Delta f & n \text{ even} \end{cases}$	$n = 0, 1, \ldots, N-1$

Two types of FDA frequency offset schemes are explored: symmetrical linear, as in [6], and alternating linear. The mathematical conventions for frequency offset definition in both scenarios are given in Table I. They are implemented using a base frequency offset of $\Delta f = 1$ MHz. The former linearly increases frequency offsets, symmetrically from the central reference antenna $n = 0$. The latter is proposed in this paper as a more optimal choice for FDA-SDF, illustrating degrees of freedom for FDA-SDF geocast delivery zone size manipulation and further precision improvements. It linearly increases the absolute value of frequency offsets, starting from the reference antenna $n = 0$ at the array edge, while alternating their sign. The benefits in FDA-SDF context of this approach are detailed throughout the remainder of this section.

Fig. 2 shows the spatial BER distribution obtained in free space for FDA-SDF using an array of $N = 3$ antennas, aligned with the y-axis and placed at the origin. For both frequency offset schemes, a geocast delivery zone, where the BER is low and information is thus retrievable, is successfully generated around the target position. It is important to note that conventional FDAs often require complex or optimization-based frequency offset definitions [7], [8] or DM extensions [10] to mitigate sidelobes of increased power (and hence decreased BER) that emerge and spread from the target position. On the other hand, FDA-SDF produces geocast delivery zones that are bounded and isolated despite the rudimentary frequency offset schemes that are employed, thus allowing to reduce the overall design complexity compared to existing FDA schemes.

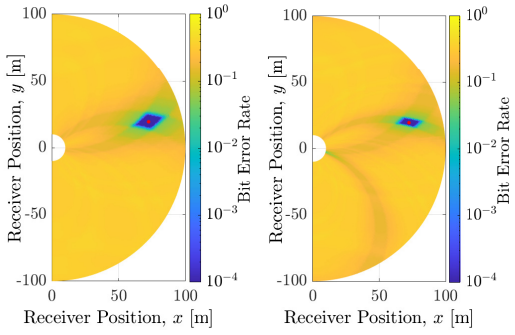

Fig. 2. FDA-SDF spatial BER distribution with $N = 3$ antennas, for symmetrical linear (left) and alternating linear (right) frequency offsets. Red dot marks target position.

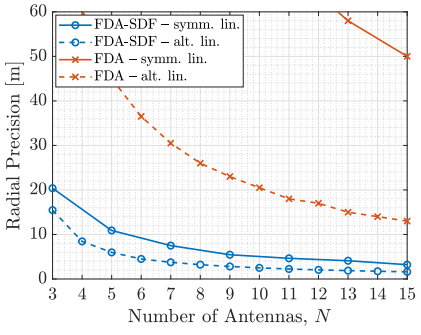

Fig. 3. Radial precision of geocast delivery zone, for varying number of antennas N.

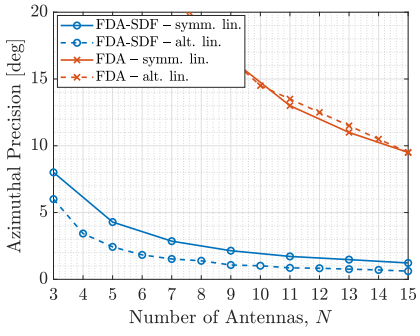

Fig. 4. Azimuthal precision of geocast delivery zone, for varying number of antennas N.

Figs. 3 and 4 evaluate the spatial precision of FDA-SDF. They show, respectively, the radial and angular width of the geocast delivery zone, where the uncoded BER remains below a threshold of 10^{-3}, as a function of the number of antennas N. These results are compared to conventional FDAs, using the same frequency offsets and array geometry.

First, these results illustrate how FDA-SDF precision is affected by frequency offset adjustments. Specifically, Fig. 3 shows that FDA-SDF radial precision is improved through the use of larger frequency offsets (as enforced for instance by the proposed alternating linear frequency offsets), and vice versa. Indeed, elevated frequency offsets Δf_n cause an increased sensitivity to the receiver radial position d of the residual phase shift (and hence symbol distortion) of the equalized symbols (8) and (12). As a result, the geocast delivery zone is narrowed along the radial axis and precision improved. This behavior is analogous to conventional FDAs, as apparent from Fig. 3 as well.
Additionally, Fig. 4 shows that FDA-SDF angular precision is improved when the reference antenna $n = 0$ is moved away from the center of the array (as in the proposed alternating linear frequency offsets for instance), and vice versa. Indeed, a reference antenna closer to the array edge ensures a larger maximal value of the delay differences $\Delta\tau_n$ between a channel and the reference one. As a result, sensitivity to the receiver azimuth position θ of the symbol distortion in (8) and (12) is increased, such that the geocast delivery zone is narrowed along the azimuth axis and precision improved. Note that this degree of freedom is novel and exclusive to FDA-SDF and hence offers an additional low-cost approach for manipulating angular precision in FDAs, simply by varying the reference antenna position in the array. Indeed, the angular precision of the conventional FDAs in Fig. 4 is identical for both frequency offset scenarios and hence invariant to the reference antenna position.

Most importantly, Figs. 3 and 4 prove FDA-SDF's superior spatial precision over conventional FDAs. Indeed, for alternating linear frequency offsets, a 3-antenna FDA-SDF setup matches the radial and angular precision of a conventional FDA using, respectively, 13 and 23 (not visible in Fig. 4) antennas. For a fair comparison, noise is added in the latter scenario such that identical SNR to the FDA-SDF scenario is obtained at the target position. At other positions, the received power and hence SNR and BER vary according to the FDA's beampattern, thus generating a geocast delivery zone of which the precision is shown in Figs. 3 and 4. Note that these results are extracted at a fixed time instance and given solely for precision comparison, as the actual FDA beampatterns, and hence geocast delivery zones, are in fact time-variant, in contrast to FDA-SDF.

V. Conclusion and Perspectives

In this paper, a novel unified frequency diverse array (FDA) and spatial data focusing (SDF) system is proposed for physical layer geocasting, i.e. spatially confined broadcasting. It overcomes beamforming and directional modulation limitations of conventional FDAs by increasing precision with reduced array size and minimal complexity. A formal FDA-based SDF (FDA-SDF) system model is presented in free space. It describes a generalized baseband approach to FDA, reducing RF resource usage, increasing frequency offset implementation flexibility, and ensuring FDA time-invariance. Additionally, dedicated SDF precoding, beamsteering, and equalization are introduced to exploit FDA multi-frequency transmission for high precision range-angle-based focusing. Simulations of the proposed scheme reveal opportunities for geocast delivery zone manipulation through simple frequency offset design and demonstrate enhanced spatial precision. In particular, it is shown that a 3-antenna FDA-SDF setup matches the radial and angular precision of a conventional FDA using, respectively, 13 and 23 antennas.

References

[1] Q. Yu and G. Heijenk, "Abiding geocast for warning message dissemination in vehicular ad hoc networks," in *ICC Workshops - 2008 IEEE International Conference on Communications Workshops*, Beijing, China, May 2008, pp. 400–404.

[2] C. Maihofer, "A survey of geocast routing protocols," *IEEE Communications Surveys & Tutorials*, vol. 6, no. 2, pp. 32–42, Second Quarter 2004.

[3] C. A. Balanis, *Arrays: Linear, Planar, and Circular*, 3rd ed. Hoboken, New Jersey, USA: John Wiley & Sons, Inc., 2005.

[4] P. Antonik, M. Wicks, H. Griffiths, and C. Baker, "Frequency diverse array radars," in *2006 IEEE Conference on Radar*, Verona, NY, USA, Apr. 2006, pp. 3 pp.–.

[5] W. Khan, I. M. Qureshi, and S. Saeed, "Frequency diverse array radar with logarithmically increasing frequency offset," *IEEE Antennas and Wireless Propagation Letters*, vol. 14, pp. 499–502, 2015.

[6] W.-Q. Wang, "DM using FDA antenna for secure transmission," *IET Microwaves, Antennas & Propagation*, vol. 11, no. 3, pp. 336–345, Feb. 2017.

[7] Y. Liu, H. Ruan, L. Wang, and A. Nehorai, "The random frequency diverse array: A new antenna structure for uncoupled direction-range indication in active sensing," *IEEE Journal of Selected Topics in Signal Processing*, vol. 11, no. 2, pp. 295–308, Mar. 2017.

[8] J. Xiong, W.-Q. Wang, H. Shao, and H. Chen, "Frequency diverse array transmit beampattern optimization with genetic algorithm," *IEEE Antennas and Wireless Propagation Letters*, vol. 16, pp. 469–472, 2017.

[9] M. P. Daly and J. T. Bernhard, "Directional modulation technique for phased arrays," *IEEE Transactions on Antennas and Propagation*, vol. 57, no. 9, pp. 2633–2640, Sep. 2009.

[10] J. Hu, S. Yan, F. Shu, J. Wang, J. Li, and Y. Zhang, "Artificial-noise-aided secure transmission with directional modulation based on random frequency diverse arrays," *IEEE Access*, vol. 5, pp. 1658–1667, 2017.

[11] G. Molineaux, S. Golstein, M. Odhiambo, F. Horlin, P. De Doncker, and J. Sarrazin, "Spatial data focusing using time and IQ resources for wireless geocasting," in *2019 IEEE Global Communications Conference (GLOBECOM)*, Waikoloa, HI, USA, Dec. 2019.

[12] G. Molineaux, M. Odhiambo, F. Horlin, P. De Doncker, and J. Sarrazin, "OFDM-based spatial data focusing for high resolution 2-dimensional wireless geocasting," in *2020 IEEE 31st Annual International Symposium on Personal, Indoor and Mobile Radio Communications*, London, United Kingdom (Great Britain), Aug. 2020, pp. 1–6.

[13] G. Molineaux, F. Horlin, P. De Doncker, and J. Sarrazin, "OFDM-based spatial data focusing for wireless physical layer geocasting in multipath channels," *IEEE Transactions on Wireless Communications*, pp. 1–1, Dec. 2021.

[14] Y. Ding, A. Narbudowicz, and G. Goussetis, "Physical limitation of range-domain secrecy using frequency diverse arrays," *IEEE Access*, vol. 8, pp. 63 302–63 309, Mar. 2020.

[15] S. Ke, M. He, X. Bu, and W. Cai, "A leakage-based directional modulation scheme for frequency diverse array in robot swarm networks," *IEEE Access*, vol. 8, pp. 107 823–107 837, Jun. 2020.